HAIT Journal of Science and Engineering B, Volume 2, Issues 3-4, pp. 452-475

Unified small-signal model for PCM control in CCM: unterminated modeling approach

Teuvo Suntio* and Mikko Hankaniemi

Institute of Power Electronics, Tampere University of Technology,
P.O. Box 692, FI-33101 Tampere, Finland
** Corresponding author: teuvo.suntio@tut.fi*

Received 1 March 2005, accepted 10 August 2005

Abstract

The small-signal modeling of peak-current-mode (PCM) controlled switched-mode converters has attracted the researchers and caused lively discussions since the invention of the control mode. The application of the PCM control makes the converter to resemble a current source at open loop rather than a voltage source, what it actually is, when the feedback loop is connected. The current-source nature has caused problems to study the converter dynamics and the anomalies it has, such as the limited duty ratio. As a consequence, generally accepted small-signal models are not available but only a variety of models serving the interests of different schools. In this paper, we will show definitively that the models including infinite duty-ratio gain form the basis for the accurate small-signal modeling as well as explain fully the phenomena characteristic to PCM control.

Keywords: Peak-current-mode control, switched-mode converter, mode limit, CCM

1 Introduction

Peak-current-mode (PCM) control was first publicly reported in 1978 [1,2] and has been a popular control method due to its inherent dynamical fea-

tures [3-5], such as pulse-by-pulse current limiting, high input-noise attenuation, and close to first-order dynamics. The main disadvantages in continuous conduction mode (CCM) are considered to be the limited duty ratio requiring compensation to extend the duty-ratio range beyond 50 %, and the noise sensitivity due to the high-bandwidth inductor-current feedback. The principles of the duty-ratio generation under PCM control are shown in Fig. 1 using a buck converter as an example. In the practical applications, the compensation ramp ($R_s M_c$) is added to the inductor-current signal ($R_s i_L$), where R_s is the equivalent inductor-current sensing resistor.

The mode limit or the maximum duty ratio, up to which the basic switching-frequency-mode operation without compensation is possible, has been considered to be the point after which the operation of the converter is unstable [1-4, 16-19]. The instability of the operation is typically proved (as in [17]) by considering the propagation of the inductor-current perturbation (Δi_L) along the successive switching cycles. It is concluded that the inductor-current perturbation may follow the rule

$$\frac{\Delta i_{Ln}}{\Delta i_{Ln-1}} = \left(\frac{d}{d'}\right)^n \tag{1}$$

which after the infinite number of cycles (i.e., $n \to \infty$) leads to an infinite inductor current, when the duty ratio (d) is greater than 0.5.

The relation in the parenthesis of (1) was originally related to the up and down slopes of the inductor current but concluded to be equal to the duty ratio and its complement in CCM. The conclusion is, however, erroneous because the slopes of the inductor current are always dependent only on the input and output voltages but not on the duty ratio. It is natural that the output voltage follows directly the duty ratio, when operating at the basic switching frequency, and as a consequence, (1) holds but its maximum value is naturally only equal to 1. The instantaneous duty-ratio relation does not hold anymore in the subharmonic modes, because the output voltage does not follow anymore the instantaneous duty ratio but the average of the instantaneous duty ratios within the cycles defined by the subharmonic order. It will be shown that the maximum value of the original ratio m_2/m_1 would stay equal to one without compensation in the subharmonic mode. It was also shown on the base of chaos theories [20] that the subharmonic operation is stable, and may occupy frequencies equal to $f_s/2^n$ (See Fig. 2), where f_s is the switching frequency and $n = 1,2,3, \ldots$, until the subharmonic number is so high that the operation becomes chaotic.

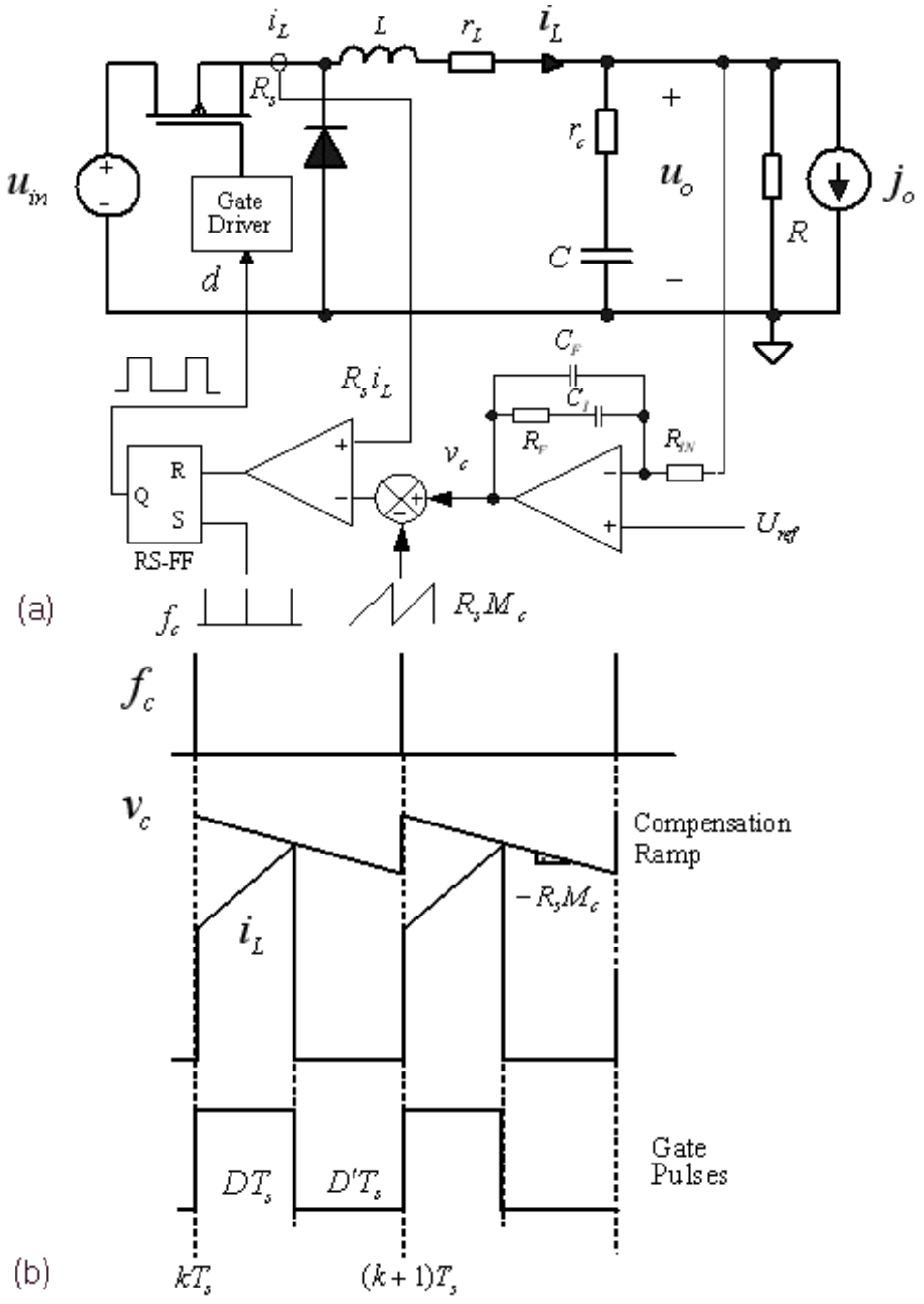

Figure 1: PCM-controlled buck converter in CCM: a) circuit schematics; b) duty-ratio generation.

The small-signal modeling technique presented in [8,9] is commonly regarded as the most accurate technique. It is based on the assumption that the origin of peculiar behavior observable during the subharmonic operation (see Fig. 2) is the sampling effect causing resonant peaking at half the switching frequency, and consequently high gain in the inductor-current loop. It is, however, so that any sampling effect has not been observed and should not theoretically exist [15] due to low-frequency eigenvalues of the circuit. It was also shown by simulation [13] that the high-frequency accuracy of the models in [8] is quite poor. The experimental frequency responses shown in [8] exhibit also poor high-frequency accuracy but the inaccuracy was claimed to be the consequence of poor grounding.

There have been numerous attempts to model the dynamical behavior of PCM-controlled converter in CCM, in addition to [8], such as [3,6,7,11-13,16,21-31] but only in discontinuous conduction mode (DCM) [9,32]. It was observed in [32] that similar phenomena as in CCM would take place also in DCM but the subharmonic mode may occupy both the even and odd subharmonics of the switching frequency. The mode limit would take place at the point where the corresponding converter would change the operating mode from DCM to CCM, respectively. The mode limit is avoided if the compensation is sufficient for the CCM operation.

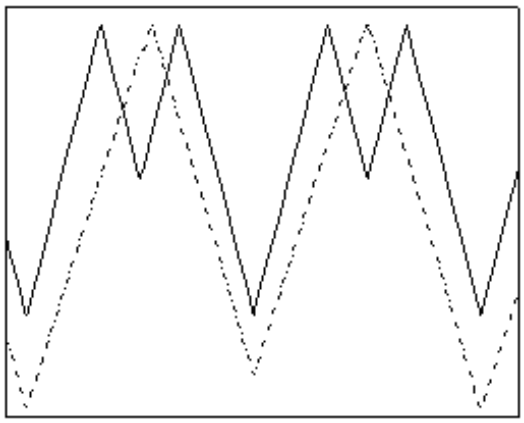

Figure 2: Simulated inductor current in the 2^{nd} (solid line) and 4^{th} (dash-dotted line) subharmonic mode without compensation.

In [25-27,30], it is proposed that the duty-ratio gain will become infinite at the mode limit irrespective of the frequency in CCM causing the peculiar behavior observed in the operation of the converter shown, e.g., in Fig. 2. This proposition is, however, widely disputed as, e.g., in [12,13,29], mainly because the existence of the extremely high gain has not been able to measure even if the clear increase in the duty-ratio gain has been observed along the increasing duty ratio [31]. The frequency-response measurement of the inductor-current loop is practically impossible, because the required loop isolation in the frequency sense cannot be fulfilled without affecting the duty-ratio generation process (Fig.1b). The high gain is, however, observable in the unterminated transfer functions, which cannot be directly measured, because the converter is a current source at open loop but may be easily computed from the measurements carried out, e.g., at a resistive load.

In [26], the high gain and the sampling effect are combined, and therefore, the resulting models would give inaccurate predictions, which have plagued the comparisons, e.g., in [12] in the favor of [8] or even led to proposing corrected models based on the sampling effect [13]. We will show in this paper that the peculiar behavior observable in the converter operation may be fully explained based on the high duty-ratio gain and, in addition, the models derived based on the high gain would give accurate predictions up to half the switching frequency.

The rest of the paper is organized as follows. The modeling technique is described in Section 2 including the general representation of the set of transfer functions for buck, boost, and buck-boost converters, as well as the effect of the transformer isolation in the case of forward, active-clamped forward and full-bridge converters. In Section 3, the origin and consequences of the mode limit are discussed and explanations are provided. In Section 4, the unterminated modeling is shortly introduced and utilized to obtain the evidence needed for the existence of high duty-ratio gain dependent only on the duty ratio. The conclusions are presented in Section 5.

The notations used in this paper are as follows. The *capital* letters denote the steady-state (DC) or *Laplace* values of the associated quantity, the *hatted small* letters denote the small-signal (ac) or *perturbed* values of the associated quantity excluding the switching ripple, the *small* letters denote the total values of the associated quantity, and the bracketed letters denote the time-varying average values of the associated quantity taken over one switching cycle, respectively.

2 Small-signal modeling

2.1 Introduction

The power stage of the associated converter does not change under PCM control, and therefore, the values of the different variables at the operating point are the same as under voltage-mode (VM) control. The only difference in the hardware sense is the generation of the duty ratio, which is based on the up slope of the inductor current (Fig.1b). Therefore, it may be obvious that the PCM control would be a direct derivative of VM control, i.e., the basic averaged and small-signal state spaces are the same but the duty ratio is no longer independent but a function of the control current, the other circuit variables and elements, respectively. The control current, denoted by i_{co}, may be presented as v_c/R_s when using the variables shown in Fig. 1a.

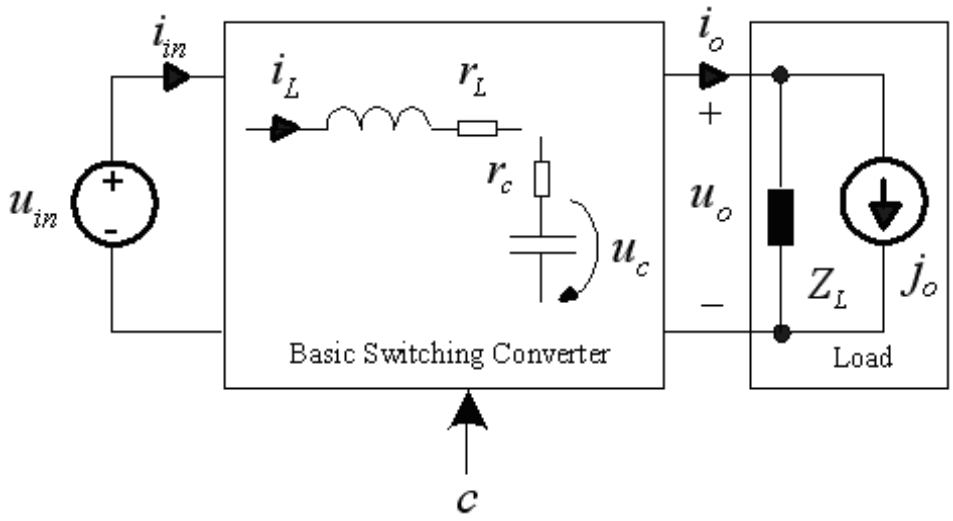

Figure 3: Definition of the variables used in the dynamical modeling of a converter.

To obtain the dynamical description for the PCM control, the functional dependence of the duty ratio on the control current, the other variables and circuit elements should be found. The small-signal functional dependence is commonly known as duty-ratio constraints [16], and presented according to (2), where the variables are defined in Fig. 3, respectively. The control current equals to c in Fig. 3.

$$\hat{d} = F_m(\hat{\imath}_{co} - q_c\hat{\imath}_L - q_o\hat{u}_o - q_i\hat{u}_{in}). \tag{2}$$

A typical procedure in obtaining the PCM state-space representation from the corresponding VM state-space representation is to replace the perturbed duty ratio with (2). It may be, however, obvious that the procedure would not be theoretically sound without replacing also the perturbed output voltage with its correct dependence on the state, input and control variables. The state-space-form constraints may be presented as

$$\hat{d} = F_m^{sp}(\hat{\imath}_{co} - q_c^{sp}\hat{\imath}_L - q_o^{sp}\hat{u}_c - q_i^{sp}\hat{u}_{in} - q_{jo}^{sp}\hat{\jmath}_o) \tag{3}$$

where the superscript '*sp*' stands for state space.

The duty-ratio constraints of (2) may be, however, used effectively, when the VM small-signal transfer functions are utilized in the control-engineering-block-diagram form modified in such a way that the small-signal inductor current is available for the feedback purposes as shown in Fig. 4. The coefficients A and B for the buck, boost, and buck-boost converters are as follows: buck– $A = 1, B = 0$, boost and buck-boost– $A = D', B = I_L$. The set of transfer functions forming the base for the dynamical characterization of a converter known also as G-parameters [36]. may be presented according to (4):

$$\begin{bmatrix} \hat{\imath}_{in} \\ \hat{u}_o \end{bmatrix} = \begin{bmatrix} Y_{in-o} & T_{ji-o} & G_{ci} \\ G_{io-o} & -Z_{o-o} & G_{co} \end{bmatrix} \begin{bmatrix} \hat{u}_{in} \\ \hat{\jmath}_o \\ \hat{c} \end{bmatrix}. \tag{4}$$

According to Fig. 4, the set of transfer functions describing the output dynamics (Fig. 4a) may be presented in a general form as (5) and for the input dynamics (Fig. 4b) as (6), respectively, where the loop gains $L_c(s)$ (i.e., inductor-current loop) and $L_v(s)$ (i.e., output-voltage loop) are defined in (7). The transfer functions denoted using the subscript extension 'v' are the corresponding VM transfer functions. Z_{L_v} is the impedance of the output capacitor connected in parallel with the load impedance Z_L (Fig. 3). The transfer functions in Fig. 4a denoted with G are naturally the transfer functions from the input and control variables to the inductor current derivable from the corresponding state space. The formalism used in presenting the transfer functions in (5) and (6) is very useful for making conclusions whether the different small-signal phenomena exist or not in the PCM controlled converter based on the knowledge of the corresponding VM controlled converter. As an example, it may be concluded that the

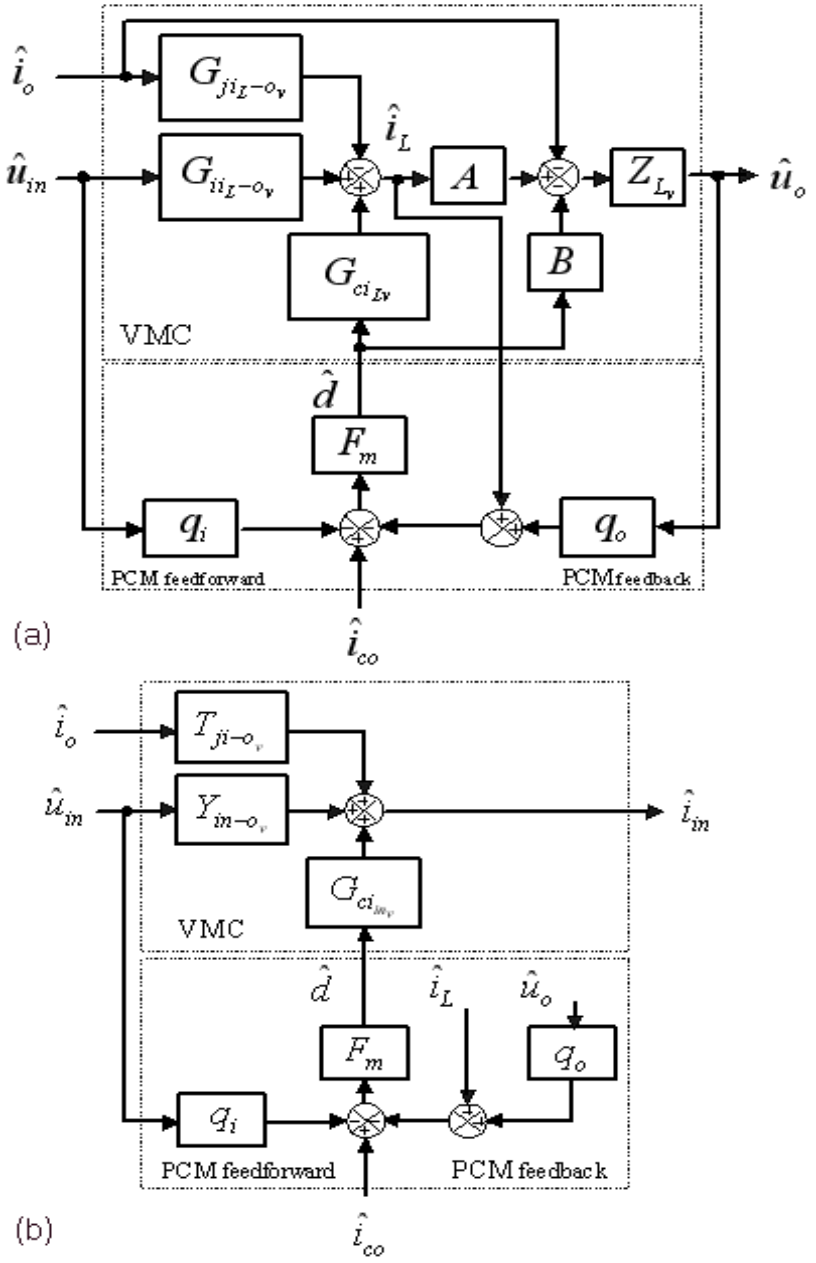

Figure 4: Block diagrams for PCM control in CCM for buck, boost and buck-boost converters: a) output dynamics; b) input dynamics.

right-hand-plane (RHP) zero existing in the VMC boost and buck-boost converters in CCM would exist similarly in the PCMC converters, according to (5).

$$
\begin{aligned}
G_{io-o} &= \frac{(1+\frac{BF_m}{A})G_{io-o_v} - F_m q_i G_{co_v}}{1+L_c(s)+L_v(s)},\\
Z_{o-o} &= \frac{(1+\frac{BF_m}{A})Z_{o-o_v} + \frac{F_m}{A}G_{co_v}}{1+L_c(s)+L_v(s)},\\
G_{co} &= \frac{F_m G_{co_v}}{1+L_c(s)+L_v(s)},
\end{aligned}
\tag{5}
$$

$$
\begin{aligned}
Y_{in-o} &= Y_{in-o_v} - \frac{F_m((q_o+\frac{1}{AZ_{L_v}})G_{io-o_v}+q_i)G_{ci_v}}{1+L_c(s)+L_v(s)},\\
T_{ji-o} &= T_{ji-o_v} + \frac{F_m((q_o+\frac{1}{AZ_{L_v}})Z_{o-o_v}-\frac{1}{A})G_{ci_v}}{1+L_c(s)+L_v(s)},\\
G_{ci} &= \frac{F_m G_{ci_v}}{1+L_c(s)+L_v(s)},
\end{aligned}
\tag{6}
$$

$$
\begin{aligned}
L_c(s) &= F_m G_{ci_{L_v}},\\
L_v(s) &= F_m G_{co_v}.
\end{aligned}
\tag{7}
$$

2.2 Duty-ratio constraints

Under PCM control, the duty ratio is generated using the up slope of the inductor current as shown in Fig. 5. The duty ratio is established, when the on-time inductor current i_L reaches the compensated control current i_{co}. It is essential to observe that the state variable is the time-varying averaged inductor current $\langle i_L \rangle$. Therefore, the comparator equation may be expressed as shown in (8), where Δi_L is the distance between the peak inductor current and the time-varying average inductor current as shown in Fig. 5. It may be obvious, according to (8), that the main task is to find the correct description for Δi_L:

$$
i_{co} - M_c d T_s = \langle i_L \rangle + \Delta i_L. \tag{8}
$$

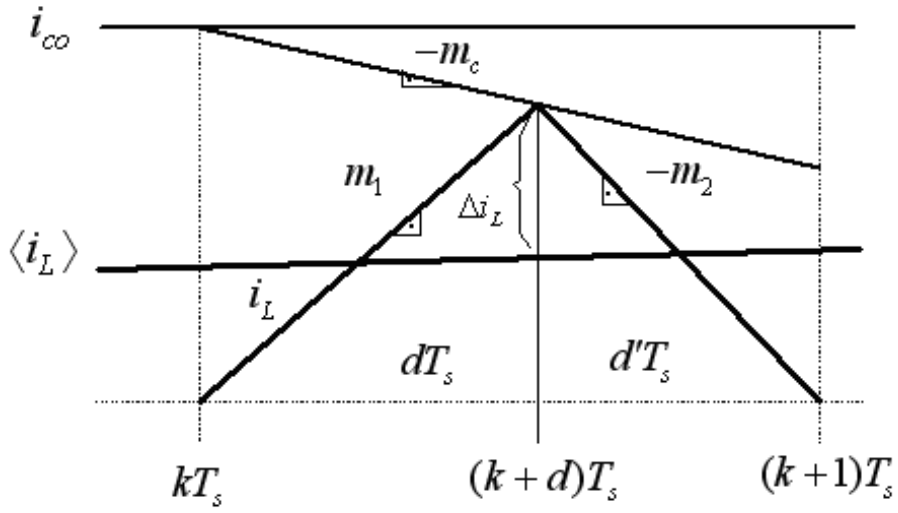

Figure 5: Duty ratio generation based on inductor current.

In CCM, the on-time and off-time inductor currents (Fig. 6) may be approximated with a first-order function of time shown in (9). The time-varying averaged inductor current may be also presented as a first-order function of time according to $\langle i_L \rangle = c_1 t + c_2$, where c_1 is the average derivative of i_{L-on} and i_{L-off}, i.e., $c_1 = dm_1 - d'm_2$ [30]. The coefficient c_2 may be found by equating the areas covered by i_L and $\langle i_L \rangle$ within a switching cycle which gives $c_2 = \dfrac{dd'T_s}{2}(m_1 + m_2) + i_L(kT_s)$. Therefore, $\langle i_L \rangle$ may be presented as shown in (10). Δi_L may be easily found computing the difference $i_{L-on}((k+d)T_s) - \langle i_L(k+d)T_s \rangle$ at $t = (k+d)T_s$, which gives (11), respectively.

$$\begin{aligned} &i_{L-on} = m_1 t + i_L(kT_s),\ kT_s \le t \le (k+d)T_s, \\ &i_{L-off} = -m_2 t + (m_1 + m_2)dT_s + i_L(kT_s),\ (k+d)T_s \le t \le kT_s, \end{aligned} \tag{9}$$

$$\langle i_L \rangle = (dm_1 - d'm_2) \cdot t + \frac{dd'T_s}{2}(m_1 + m_2) + i_L(kT_s), \tag{10}$$

$$\Delta i_L = \frac{dd'}{2} \cdot (m_1 + m_2). \tag{11}$$

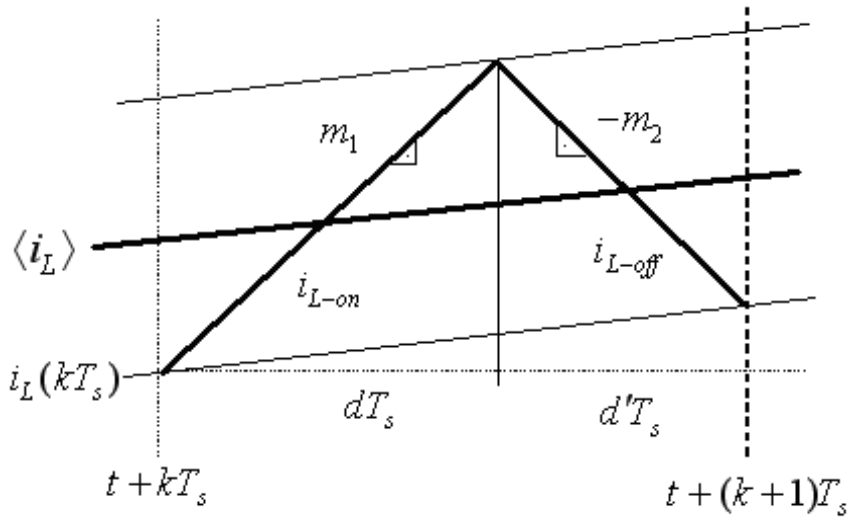

Figure 6: Inductor current waveforms.

Implicitly the same value for Δi_L (11) is obtained in [25] by inspecting the inductor current waveforms, and in [27] using the theoretical averaging method known as KBM method [15]. In [26], the same value is used but its origin is not clearly stated. When (11) is inserted into (8), we obtain the averaged duty-ratio constraints (12) from which the small-signal constraints (2) and (3) may be derived by replacing the topology-based up and down slopes and developing the proper partial derivatives:

$$i_{co} - M_c dT_s = \langle i_L \rangle + \frac{dd'}{2} \cdot (m_1 + m_2). \tag{12}$$

The corresponding coefficients are shown in Table 1 (2) and Table 2 (3) for the buck, boost, and buck-boost converters, respectively. The coefficients in Table 2 are presented in such a way that the effect of load impedance is removed, i.e., in an unterminated mode, which is explained in more detail in Section 4. The PCMC transfer functions may be obtained from (5) and (6) by replacing the corresponding coefficients with those defined in Table 1. It may be obvious that, according to Tables 1 and 2, the duty-ratio gain F_m would become infinite at $D = 50\%$ without compensation (i.e., $M_c = 0$). The maximum duty ratio, when a certain amount of compensation is applied, may be presented in a general form as

$$D_{\max} = 0.5 + \frac{M_c}{M_1 + M_2} \tag{13}$$

	F_m	q_c	q_o	q_i
Buck	$\frac{1}{T_s(M_c + \frac{(D'-D)(U_{in}+U_D)}{2L})}$	1	0	$\frac{DD'T_s}{2L}$
Boost	$\frac{1}{T_s(M_c + \frac{(D'-D)(U_o+U_D)}{2L})}$	1	$\frac{DD'T_s}{2L}$	0
Buck-boost	$\frac{1}{T_s(M_c + \frac{(D'-D)(U_{in}+U_o+U_D)}{2L})}$	1	$\frac{DD'T_s}{2L}$	$\frac{DD'T_s}{2L}$

Table 1. Coefficients of duty-ratio constraints in (2).

	F_m^{sp}	q_c^{sp}	q_o^{sp}	q_i^{sp}	q_{io}^{sp}
Buck	$\frac{1}{T_s(M_c+\frac{(D'-D)(U_{in}+U_D)}{2L})}$	1	0	$\frac{DD'T_s}{2L}$	0
Boost	$\frac{1}{T_s(M_c+\frac{(D'-D)(\frac{r_cDI_o}{D'}+U_o+U_D)}{2L})}$	$1+\frac{r_cDD'T_s}{2L}$	$\frac{DD'T_s}{2L}$	0	$-\frac{r_cDD'T_s}{2L}$
Buck-boost	$\frac{1}{T_s(M_c+\frac{(D'-D)(\frac{r_cDI_o}{D'}+U_{in}+U_o+U_D)}{2L})}$	$1+\frac{r_cDD'T_s}{2L}$	$\frac{DD'T_s}{2L}$	$\frac{DD'T_s}{2L}$	$-\frac{r_cDD'T_s}{2L}$

Table 2. Coefficients of duty-ratio constraints in (3)

2.3 Effect of transformer isolation

Transformer isolation is often used for safety reasons and/or for scaling the input voltage to obtain more optimal duty-ratio range [33,34]. The inductor-current feedback is commonly taken from the transformer primary current containing the reflected secondary inductor current and the magnetizing current of the transformer as shown in Fig. 7 in the case of a single-ended forward converter. It may be obvious that the magnetizing current may have a similar effect as the artificial compensation.

Consequently, the effect of magnetizing inductance on the duty-ratio constraints may be considered similarly to the artificial compensation giving the comparator equation (2), as shown in (14) for buck derived converters, where $L_{M1} = \left(\frac{N_2}{N_1}\right)^2 \cdot L_M$, $u_{in1} = \frac{N_2}{N_1} \cdot u_{in}$, and k is a scaling factor dependent on the transformer reset mechanism: $k = 1$ for single and double ended forward; $k = 1/2$ for active-clamped forward [35] and full-bridge [16]:

$$i_{co} - M_c dT_s - \frac{k u_{in1} dT_s}{L_{M1}} = \langle i_L \rangle + \frac{dd' T_s u_{in1}}{2L}. \tag{14}$$

By taking proper partial derivatives, we may compute from (14) the duty-ratio-constraints coefficients shown in (15). It may be obvious that the active duty-ratio range would be extended beyond 50 % (16) depending on the reset mechanism and the ratio between the inductance values of the output inductor and the magnetizing inductor without the artificial compensation.

$$\begin{aligned} F_m &= \frac{1}{T_s(M_c + \frac{kU_{in1}}{2L_{M1}} + \frac{(D'-D)U_{in1}}{2L})}, \\ q_c &= 1, \\ q_o &= 0, \\ q_i &= \frac{kDT_s}{2L_{M1}} + \frac{DD'T_s}{2L}, \end{aligned} \tag{15}$$

$$D_{\max} = 0.5 + \frac{kL}{2L_{M1}}. \tag{16}$$

3 Origin and consequences of mode limit

The duty-ratio constraints of (12) may be also presented at the steady state as shown in (17). We may compute from (17) that $I_{co} - I_L$ may be presented

in respect to the steady-state duty ratio as shown in (18), which clearly has a minimum at $D = 0.5 + \dfrac{M_c}{M_1 + M_2}$:

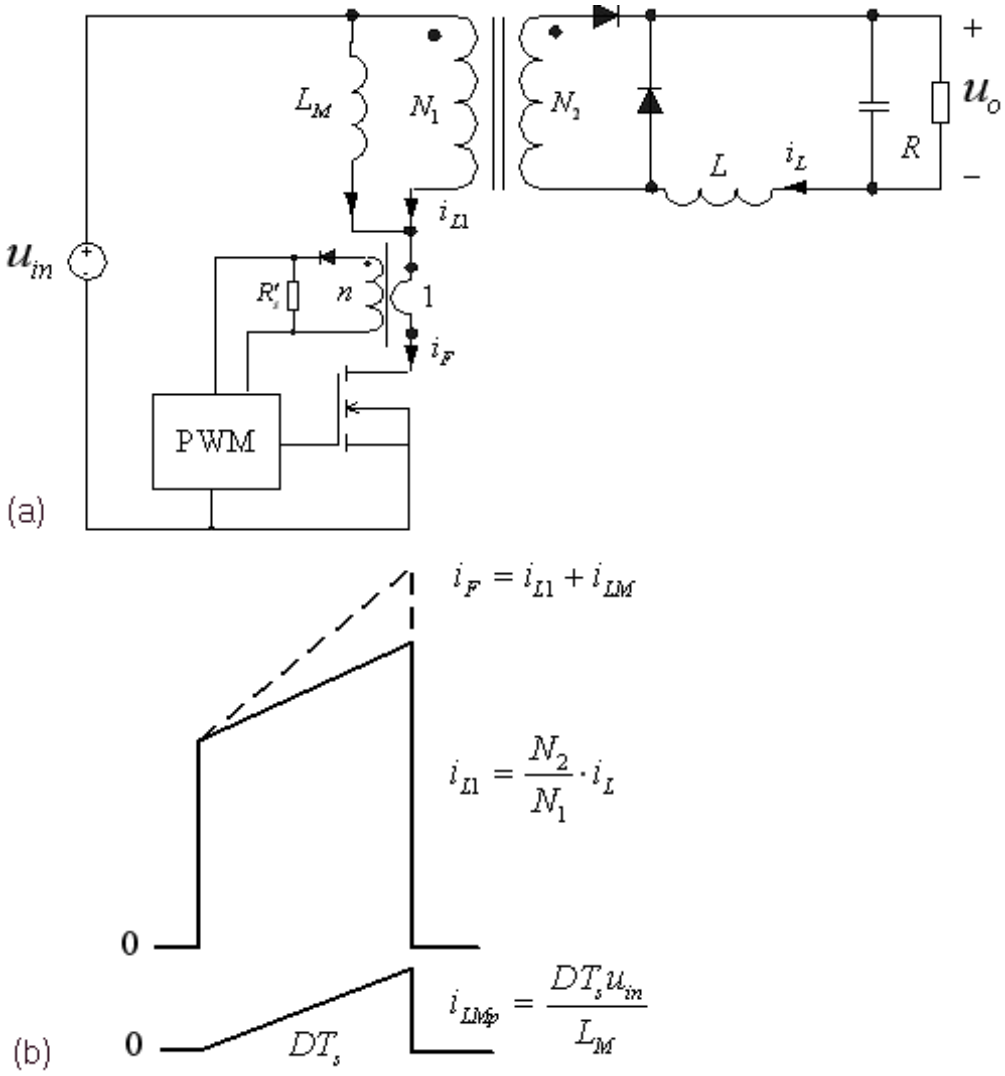

Figure 7: Single-ended forward converter: a) circuit schematics without reset winding; b) primary-side switch current.

$$I_{co} - I_L = -\frac{(M_1 + M_2)T_s}{2} \cdot D^2 + (M_c + \frac{M_1 + M_2}{2})T_s \cdot D, \tag{17}$$

$$(I_{co} - I_L)_{\min} = \frac{M_c T_s}{2}(1 + \frac{M_c}{M_1 + M_2}) + \frac{(M_1 + M_2)T_s}{8}. \tag{18}$$

The duty ratio corresponding to the minima (18) is exactly the same as the maximum duty ratio defined in (13) at which the small-signal duty-ratio gain F_m would become infinite. The shape of the difference $I_{co} - I_L$ dictates that it would decrease along the increasing duty ratio up to the mode limit after which it should start decreasing again. It is, however, impossible in practice, because the increasing duty ratio would further decrease the peak-to-peak inductor-current ripple. We may also develop (17) in terms of D, as shown in (19), having solution shown in (20). If $I_{co} - I_L$ in (20) is replaced with the minima (18), the term inside the square root becomes equal to zero, i.e., the real valued solutions exist only up to $D_{\max}$ (13).

$$D^2 - (1 + \frac{2M_c}{M_1 + M_2})D + \frac{2(I_{co} - I_L)}{T_s(M_1 + M_2)} = 0, \tag{19}$$

$$D = \frac{1}{2}(1 + \frac{2M_c}{M_1 + M_2}) - \sqrt{\frac{1}{4}\left(1 + \frac{2M_c}{M_1 + M_2}\right)^2 - \frac{2(I_{co} - I_L)}{T_s(M_1 + M_2)}}. \tag{20}$$

It is observed that the behavior of the PCM controlled converter is peculiar after the mode limit: the inductor current up and down slopes maintain a certain relation (Fig. 8) and the ideal modulo $M(D)$ behaves as if the duty ratio were equal to $D_{\max}$ defined in (13).

The observed peculiar behavior at open loop may be explained in such a way that the infinite duty-ratio gain F_m forces the derivative of the average inductor current (i.e., $dm_1 - d'm_2$ [30]) to be zero, because the small-signal control current is zero at open loop. At the mode limit $d = D_{\max}$, and therefore, $D_{\max}M_1 - D'_{\max}M_2 = 0$ giving (21). If $D_{\max}$ in (21) is replaced with (13), we will get (22). The relation in (21) defines that the up and down slopes are equal when $M_c = 0$, as may be easily observed from Fig. 8a. When compensation is applied, the relation between the slopes is

$$\frac{M_1}{M_2} = \frac{D'_{\max}}{D_{\max}}, \tag{21}$$

$$M_1 = M_2 + 2M_c. \tag{22}$$

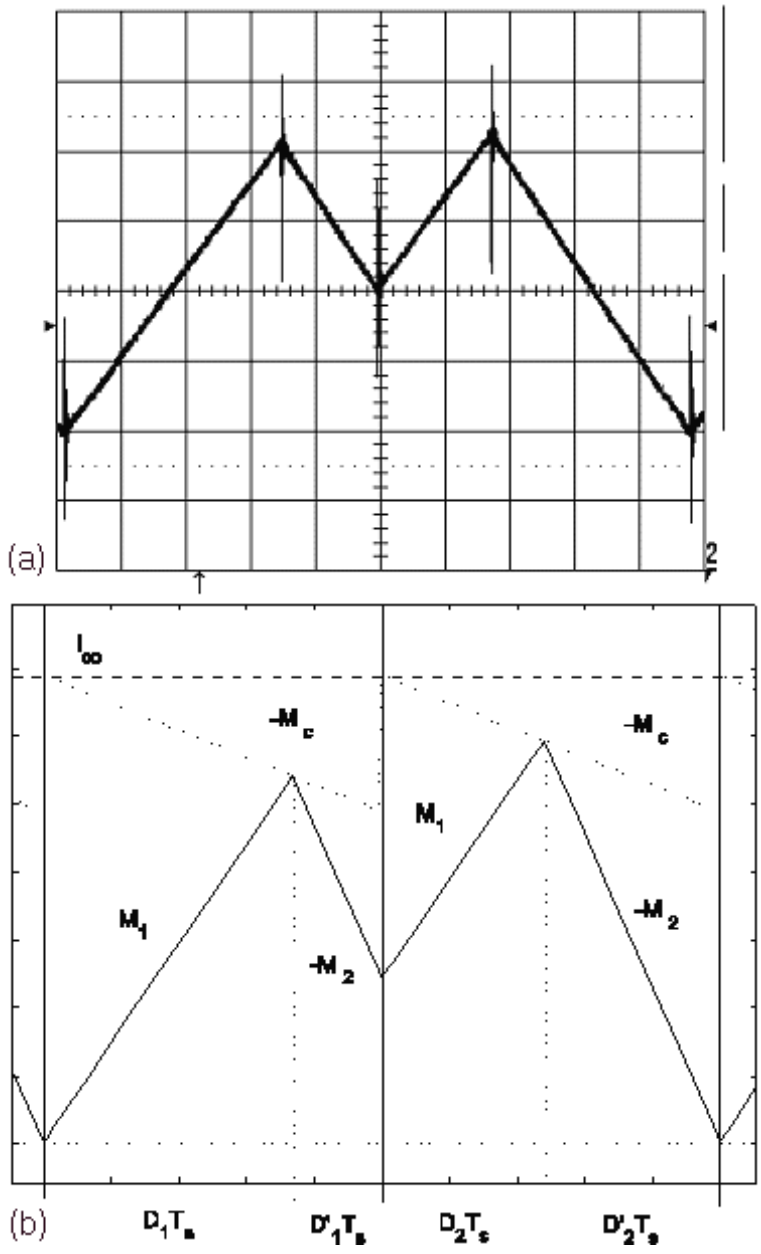

Figure 8: Inductor-current waveforms in subharmonic mode: a) measured inductor-current waveforms in the second harmonic mode without compensation; b) simulated inductor-current waveforms in the second harmonic mode with a certain amount of compensation.

According to Fig. 8b, we may compute that

$$\begin{aligned}(M_1 + M_c)D_1 &= M_2 D_2' + M_c D_2 \\ (M_1 + M_c)D_2 &= M_2 D_1' + M_c D_1\end{aligned} \tag{23}$$

$$\frac{D_1 + D_2}{2} = \frac{M_2}{M_1 + M_2}. \tag{24}$$

Eq. (24) defines the average duty ratio D_{av} in the second-subharmonic mode. If we denote by $M = \frac{U_o}{U_{in}}$, and consider the ideal converters, then, according to (24), we will get for a buck converter $M = D_{av}$, for a boost converter $M = \frac{1}{D'_{av}}$, and for a buck-boost converter $M = \frac{D_{av}}{D'_{av}}$, which are similar to the ideal modulos defined, e.g., in [16]. We may compute that $D_{av} = D_{\max}$ defined in (13).

4 Unterminated modeling

The set of transfer functions (4) is typically derived using a resistive load (i.e.,$Z_L = R$, Fig. 9). Most often, the impedance-type load is not known in the practical applications, and it may vary. Therefore, it may be obvious that the dynamic model of a converter should be one from which the load effect is removed. Such a model is known as an unterminated model [30]. The unterminated transfer functions may be derived assuming the converter to be loaded only with a constant-current-type load (i.e., i_o in Fig. 9). The dynamics associated to a converter may be presented using a two-port model equivalent to the set of transfer functions in (4). In an unterminated mode, the two-port model may be given as shown in Fig. 9, where the superscript '*' denotes the unterminated nature of the corresponding transfer functions [30].

The load effect may be added to the output dynamics computing $\hat{u}_o$ from Fig. 9 at the presence of the load giving

$$\hat{u}_o = \frac{G^*_{io-o} \cdot \hat{u}_{in} - Z^*_{o-o} \cdot \hat{j}_o + G^*_{co} \cdot \hat{c}}{1 + \frac{Z^*_{o-o}}{Z_L}} \tag{25}$$

The load effect on the input dynamics may be found computing $\hat{i}_o$ at the output side and replacing it in the input side by means of the computed formula. We are only interested in the output dynamics, and therefore, we do not present the formulation to the input dynamics but it may be found from [30].

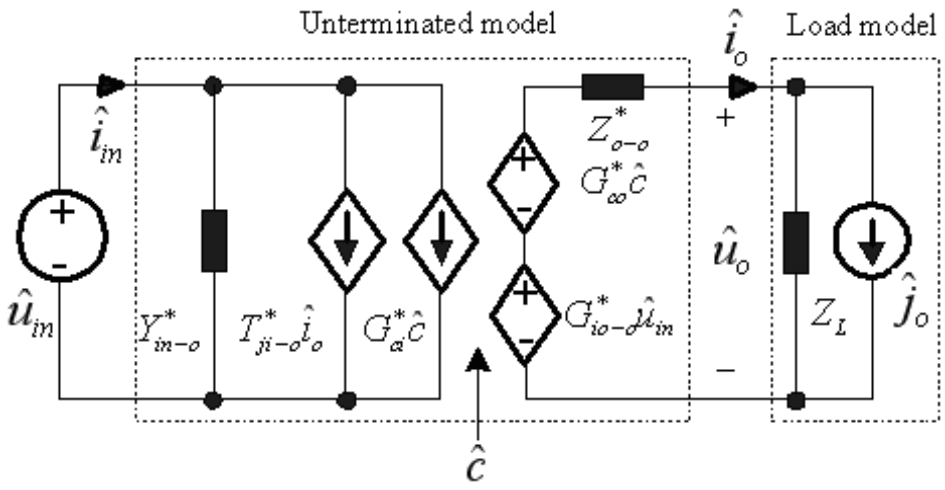

Figure 9: Two-port model of a converter and a load.

The unterminated transfer functions may be measured also in practice using frequency-response analyzers, when the converter is loaded with a constant-current load. A PCM controlled converter is, however, a current source at open loop, and therefore, it does not operate at a constant-current load properly but the load has to be, e.g., a resistor. At resistive load, the increase in the duty-ratio gain, when approaching the mode limit, may not be clearly observable due to the effect of the resistive load. Eq. (25) would, however, provide a method to compute the unterminated transfer functions, where the effect is clearly visible, from the measured transfer functions. The unterminated control-to-output transfer function G^*_{co} and the open-loop output impedance Z^*_{o-o} would show the effect especially at the low frequencies, where the magnitude would increase and the low-frequency pole would move closer to the origin, when the duty ratio approaches the mode limit, i.e., 50 %. The moving of the high-frequency pole of G^*_{co} closer to the infinity may be also observable from the phase behavior but may be hardly measured accurately in practice. G^*_{co} and Z^*_{o-o} may be computed from the measured G_{co} and Z_{o-o} as

$$\begin{aligned} Z^*_{o-o} &= \frac{RZ_{o-o}}{R - Z_{o-o}}, \\ G^*_{co} &= \frac{G_{co}}{Z_{o-o}} \cdot Z^*_{o-o}. \end{aligned} \tag{26}$$

G^*_{co} and Z^*_{o-o} of an ideal buck converter in CCM are shown in (27),

and the corresponding terminated transfer functions, respectively, in (28). According to (27), it may be obvious that the maximum gain of G^*_{co} and Z^*_{o-o} is equal to $F_m U_{in}$ providing the evidence of high duty-ratio gain if existing. According to (28), the maximum gain of G_{co} and Z_{o-o} is equal to R, which may be difficult to interpret directly as an evidence of the existing high duty-ratio gain.

$$\begin{aligned} G^*_{co} &= \frac{\frac{F_m U_{in}}{LC}}{s^2 + s\frac{F_m U_{in}}{L} + \frac{1}{LC}}, \\ Z^*_{o-o} &= \frac{\frac{F_m U_{in} + sL}{LC}}{s^2 + s\frac{F_m U_{in}}{L} + \frac{1}{LC}}, \end{aligned} \tag{27}$$

$$\begin{aligned} G_{co} &= \frac{\frac{F_m U_{in}}{LC}}{s^2 + s(\frac{F_m U_{in}}{L} + \frac{1}{RC}) + \frac{F_m U_{in} + R}{LCR}}, \\ Z_{o-o} &= \frac{\frac{F_m U_{in} + sL}{LC}}{s^2 + s(\frac{F_m U_{in}}{L} + \frac{1}{RC}) + \frac{F_m U_{in} + R}{LCR}}. \end{aligned} \tag{28}$$

The frequency responses of the terminated control-to-output transfer function and the open-loop output impedance of an ideal buck converter operating at 100 kHz at a resistive load were simulated, and the gain and phase of the responses were extracted from the response data using the fast Fourier transformation (FFT). The corresponding unterminated responses were computed using (26). The frequency responses of the unterminated control-to-output transfer function, when the duty ratio approaches the mode limit (i.e., $D = 0.3857, 0.4639, 0.4889, 0.4942$), are shown in Fig. 10a for the frequencies from 1 Hz to 100 kHz. The simulated responses are denoted using a dot. The lowest and highest excitation frequencies were 3 Hz and 30 kHz, respectively. The effect of the increasing duty-ratio gain is best observable as the low-frequency phase behavior but also visible at the high-frequency phase behavior as well as at the low-frequency gain. The frequency responses of the unterminated open-loop output impedance are shown in Fig. 10b for the frequencies from 0.1 Hz to 100 Hz. The simulated frequency responses at 3 Hz and 10 Hz are denoted using a dot. The effect

of the increasing duty-ratio gain is clearly visible. The predictions and the switching-model frequency responses match each other extremely well.

5 Conclusions

The small-signal modeling of a PCM controlled converter would be a direct derivative of a corresponding direct-duty-ratio or VM controlled converter. The small-signal state space of a PCM controlled converter may be obtained from the corresponding VM state space by replacing the perturbed duty ratio with the duty-ratio constraints describing the functional dependence of the duty ratio on the control current and other variables, as well as circuit elements. The derived duty-ratio gain would exhibit infinite gain at the mode limit, as already has been proposed several times earlier. The possible existence of the frequency-independent high gain has been disputed because of inability to measure the high gain. We showed in this paper that the high gain is clearly visible in the unterminated transfer functions, which cannot be directly measured using a constant-current load at open loop but may be computed from the responses measured, e.g., at a resistive load. The infinite gain would also explain the peculiar behavior observed at open loop and provide useful information for the analysis and design of the PCM controlled converters.

References

[1] C.W. Deisch, IEEE Power Electronics Specialists Conference, PESC'78, p.300 (1978).

[2] A. Capel, G. Ferrante, D. O'Sullivan, and A. Weinberg, IEEE Power Electronics Specialists Conference, PESC'78, p.135 (1978).

[3] S-H. Hsu, A. Brown, L. Rensink, and R.D. Middlebrook, IEEE Power Electronics Specialists Conference, PESC'79, p.248 (1979).

[4] R. Redl and N.O. Sokal, IEEE Power Electronics Design Conference, p.18 (1985).

[5] R. Redl and N.O. Sokal, IEEE Trans. on Power Electronics **1**, 181 (1986).

[6] R.D. Middlebrook, IEEE Trans. on Power Electronics **4**, 36 (1989).

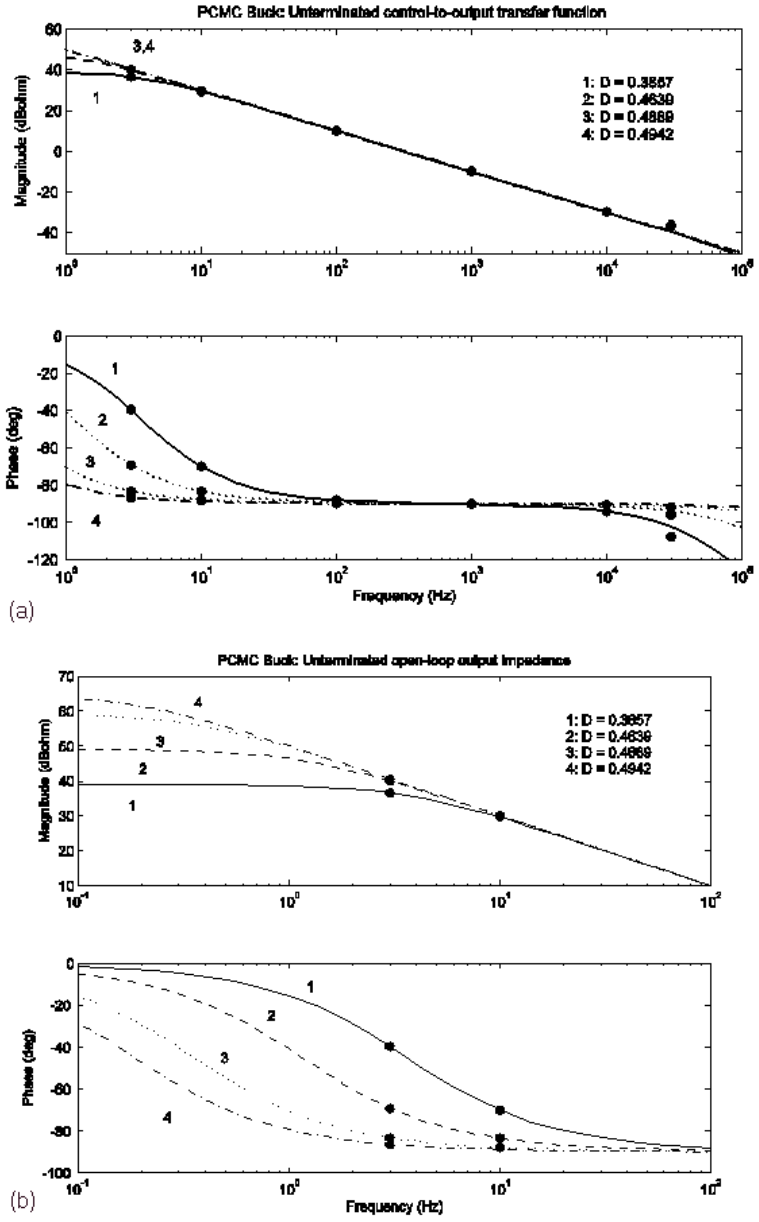

Figure 10: Measured and predicted frequency responses of a buck converter, when the duty ratio approaches the mode limit. a) G_{co}^{*} at $D = 0.3857, 0.4639, 0.4889, 0.4942$; b) Z_{o-o}^{*} at $D = 0.3857, 0.4639, 0.4889, 0.4942$.

[7] G.C. Verghese, C.A. Bruzos, and K.N. Mahabir, IEEE Power Electronics Specialists Conference, PESC'89, p.484 (1989).

[8] R.B. Ridley, IEEE Trans. on Power Electronics **6**, 271 (1991).

[9] R.B. Ridley, IEEE Power Electronics Specialists Conference, PESC'90, p.382 (1990).

[10] Y-S. Jung, I-H. Oh, H-C. Choi and M-J. Youn, International Journal of Electronics **86**, 391 (1999).

[11] W-H. Ki, IEEE Trans. on Circuits and Systems-I **45**, 104 (1998).

[12] Y-W. Lo and R.J. King, IEEE Trans. on Power Electronics **14**, 918 (1999).

[13] B. Johansson, IEEE Telecommunication Energy Conference INTELEC'02, p.552 (2002).

[14] D.M. Mitchell, IEEE Trans. on Aerospace and Electronic Systems **16**, 272 (1980).

[15] R.M. Bass, *Large-Signal Tools for Power Electronics: State-Space Analysis and Averaging Theory*, Ph. D Dissertation, University of Illinois at Urbana Campaign, 1990.

[16] R.W. Erickson and D. Maksimovic, *Fundamentals of Power Electronics,* 2-nd ed. (Kluwer Academic Publishers, 2001).

[17] A.S. Kislovski, IEEE Applied Power Electronics Conf. APEC'91, p. 459 (1991).

[18] S. Paljasevic and D. Maksimovic, IEEE Power Electronics Specialists Conference, PESC'97, p.1323 (1997).

[19] I. Zafrany and S. Ben-Yakov, IEEE Power Electronics Specialists Conference, PESC'95, p.1111 (1995).

[20] S. Banerjee and G.C. Verghese, *Nonlinear Phenomena in Power Electronics* (IEEE Press, NJ, USA, 2001).

[21] D.J. Perrault and G.C. Verghese, IEEE Trans. on Power Electronics **12**, 453 (1997).

[22] F.R. Rodriquez and J.E. Chen, IEEE Trans. on Power Electronics **6**, 656 (1991).

[23] V. Vorperian, IEEE Trans. on Aerospace and Electronic Systems **26**, 490 (1990).

[24] R. Tymerski and D. Li, IEEE Trans. on Power Electronics **8**, 271 (1993).

[25] C.P. Schultz, Proc. Power Conversion and Intelligent Motion PCIM'93, p.319 (1993).

[26] F.D. Tan and R.D. Middlebrook, IEEE Trans. on Power Electronics **10**, 397 (1995).

[27] J. Sun and R.M. Bass, Proc. IEEE Industrial Electronics Society Conference, IECON'97, p. 599 (1997).

[28] C-C. Fang and E.H. Abed, International Journal of Electronics **88**, 347 (2001).

[29] M.K. Kazimierczuk, IEEE Trans. on Circuits and Systems-I **47**, 1407 (2000).

[30] T. Suntio, IEEE Industrial Electronics Society Conference, IECON'02, p.1398 (2002).

[31] S-S. Hong, B. Choi, and H-S. Ahn, J. of Circuits, Systems and Computers **13**, 725 (2004).

[32] T. Suntio, IEEE Trans. on Industrial Electronics **48**, 127 (2001).

[33] T. Suntio, J. Lempinen, I. Gadoura, and K. Zenger, Proc. IEEE Nordic Workshop on Power and Industrial Electronics (NORPIE) Record, p.180 (2000).

[34] R.B. Ridley, Proc. Unitrode Power Supply Design Seminar, SEM-1300, p.A2-1 (2000).

[35] H.K. Ji and H.J. Kim, IEEE Power Electronics Specialists Conference, PESC'94, p.895 (1994).

[36] T. Suntio and I. Gadoura, IEEE Telecommunication Energy Conference, INTELEC'02, p.560 (2002).